

Impact of LIGO-Virgo binaries on gravitational wave background searches

Marek Lewicki^{1,*} and Ville Vaskonen^{2,†}

¹*Faculty of Physics, University of Warsaw ul. Pasteura 5, 02-093 Warsaw, Poland*

²*Institut de Física d'Altes Energies (IFAE), The Barcelona Institute of Science and Technology, Campus UAB, 08193 Bellaterra (Barcelona), Spain*

We study the impact of the binary population currently probed by LIGO-Virgo on future searches for the primordial gravitational wave background. We estimate the foreground generated by the binaries using the observed event rate and a simple modeling of the black hole population. We subtract individually resolvable binaries from the foreground and utilize Fisher analysis to derive sensitivity curves similar to the power-law integrated prescription. We find that despite this improved treatment the reach of future experiments will still be severely impacted.

Introduction – Various cosmological processes may have generated gravitational waves (GWs) that contribute to the stochastic GW background [1]. If this background is sufficiently strong, it can be probed with GW detectors. The non-observation of such background with LIGO-Virgo detectors has been translated into mild constraints on the possible cosmological GW sources [2–4]. As shown in Fig. 1, many new experimental programs, built on the success of currently running LIGO-Virgo network, are expected to enter GW search in the next decades. With tremendous sensitivity improvements, these experiments will further probe the early Universe processes that can generate GWs.

The LIGO-Virgo detectors have observed dozens of GW signals from compact object mergers [5–7]. From these observations we now have a good understanding of the population of $\mathcal{O}(10M_\odot)$ black holes (BHs) and their present merger rate, and therefore we can estimate how strong astrophysical GW foreground these binary BHs (BBHs) generate. This foreground will impact the detectability of the primordial GW background with future GW experiments. We will present a simple analysis quantifying the effect of the BBH foreground on searches of the primordial GW background. Another astrophysical foreground which is known to have an impact on the reach of GW experiments comes from binary white dwarfs (BWDs) [8, 9]. We will include this foreground in our analysis as modeled for the LISA experiment in [10, 11].

The problem of probing the primordial GW background in the presence of an astrophysical foreground has been recently studied in several papers (see e.g. [12–19]). Our analysis improves over the earlier studies by systematically subtracting the resolvable BH binaries from the total foreground, and by accounting for the uncertainties in the BBH merger rate, which translate into priors for the amplitude of the GW foreground. We quantify, using Fisher analysis, what impact this foreground will have on detection of primordial GW backgrounds modeled in the simplest and most generic case as power-laws. We find that subtracting the identified binaries can significantly mitigate the foreground especially for experi-

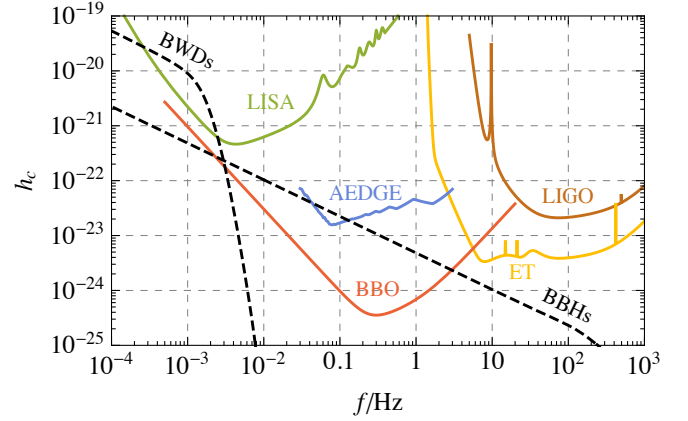


FIG. 1. The design GW strain sensitivities of LIGO [20], ET [21], LISA [11, 22], AEDGE [23, 24] and BBO [25]. The black dashed curves show the GW foregrounds from binary white dwarfs (BWDs) and from $\mathcal{O}(10M_\odot)$ binary black holes (BBHs).

ments with sensitivity to probe signals far weaker than the foreground itself. However, the sensitivity of all experiments will still be severely impacted, limiting their reach in probing of primordial GW sources.

BBH merger rate – Assuming that the BH population that LIGO-Virgo is probing is astrophysical, we use a truncated power-law mass function and a merger rate that follows the star formation rate with a power-law delay time distribution distribution. The differential BBH merger rate then is of the form

$$\frac{dR(t)}{dm_1 dm_2} = \frac{R_0}{Z_\psi} M^\alpha \eta^\beta \psi(m_1) \psi(m_2) \times \int dt_d dz_b P_b(z_b) P_d(t_d) \delta(t - t(z_b) - t_d), \quad (1)$$

where the normalization factor Z_ψ is defined such that $R = R_0$ at $z = 0$, $M = m_1 + m_2$ and $\eta = m_1 m_2 / M$ are the total mass and the symmetric mass ratio of the binary, and the mass dependence of the binary population is parametrized by α and β . The function $P_b(z)$ is given

by the star formation rate [26],

$$\text{SFR}(z) \propto \frac{(1+z)^{2.6}}{1 + ((1+z)/3.2)^{6.2}} \equiv P_b(z), \quad (2)$$

and for the time delay distribution we use $P_d(t) \propto t^{-1}$ at $t > 50 \text{ Myr}$ [27]. The mass function is

$$\psi(m) \propto m^\zeta \theta(m - m_{\min}) \theta(m_{\max} - m), \quad (3)$$

with the normalization $\int \psi(m) d \ln m = 1$. We take $m_{\min} = 3.0 M_\odot$ and $m_{\max} = 55 M_\odot$ corresponding to the estimates for the maximal mass of neutron stars and the beginning of the pair instability mass gap. We use the values $\alpha = 0$, $\beta = 6$, $\zeta = -0.5$ and $R_0 = 10_{-5}^{+6} \text{ Gpc}^{-3} \text{ yr}^{-1}$, following the fit performed in [28] to the LIGO-Virgo observations. For indicative errors or the resulting stochastic GW foreground, we include the uncertainties only for the present merger rate R_0 and use the central values for the other parameters.

Detectability of individual BBHs – The amplitude $|\tilde{h}(f)|$ of the Fourier transform of the inspiral-merger-ringdown GW signal from a BBH can be approximated as [29]

$$|\tilde{h}(f)| = \sqrt{\frac{5\eta}{24}} \frac{[GM(1+z)]^{5/6}}{\pi^{2/3} D_L} \times \begin{cases} f^{-7/6}, & f < f_{\text{merg}}, \\ f_{\text{merg}}^{-1/2} f^{-2/3}, & f_{\text{merg}} \leq f < f_{\text{ring}}, \\ f_{\text{merg}}^{-1/2} f_{\text{ring}}^{-2/3} \frac{\sigma^2}{4(f - f_{\text{ring}})^2 + \sigma^2}, & f_{\text{ring}} \leq f < f_{\text{cut}}, \end{cases} \quad (4)$$

where M , η , z and D_L are the total mass, the symmetric mass ratio, the redshift and the luminosity distance of the BBH, and the frequencies f_{merg} , f_{ring} , f_{cut} and σ are of the form

$$f_j = \frac{a_j \eta^2 + b_j \eta + c_j}{\pi G M (1+z)}, \quad (5)$$

with the coefficients a_j , b_j and c_j given in Table I of Ref. [29].

The signal-to-noise ratio $\text{SNR}(f)$ of a BBH signal depends on the orientation of the detector with respect to the sky location of the binary and on the inclination of the binary. For an optimally oriented binary-detector system, neglecting the rotation of the detector, the signal-to-noise ratio of the BBH signal that in the end of the experiment is at frequency f , or the BBH has merged, is given by

$$\text{SNR}(f) = \sqrt{4 \int_{f(\mathcal{T} + \tau(f))}^f df' \frac{|\tilde{h}(f')|^2}{S_n(f')}}}, \quad (6)$$

where S_n is the noise power spectrum of the GW detector, that includes the instrumental noise and the GW foregrounds from WDBs and BBHs. The characteristic

strain from these noise components is shown in Fig. 1, and the BBH contribution is described in the next section. The lower integration limit depends on the duration of the experiment, \mathcal{T} , and the coalescence time of the binary,

$$\tau(f) = \frac{(5/\tau)^{3/8}}{8\pi \eta^{3/8} [(1+z)M]^{5/8}}. \quad (7)$$

Throughout this paper for all experiments we assume a duration of $\mathcal{T} = 4 \text{ yr}$.

We estimate how large fraction of the BBH signals can be resolved by calculating the probability [30]

$$p_{\text{det}}(f) = \int_{r(f)}^1 p(\omega) d\omega, \quad (8)$$

where $r(f) = \text{SNR}_c / \text{SNR}(f)$, that accounts for the antenna patterns $F_{+, \times}$ of the detector and averages over the binary sky location and inclination, and the polarization of the signal. The parameter ω is defined as

$$\omega = \sqrt{\frac{(1 + c_i^2)^2}{4} F_+(\theta, \phi, \psi)^2 + c_i^2 F_\times(\theta, \phi, \psi)^2}, \quad (9)$$

and its probability distribution $p(\omega)$ is calculated assuming uniform distributions for the binary inclination $c_i \in (-1, 1)$, sky location $\cos \theta \in (-1, 1)$ and $\phi \in (0, 2\pi)$, and the polarization angle $\psi \in (0, 2\pi)$. We use $\text{SNR}_c = 8$ as the threshold value for the signal-to-noise ratio.

GW foreground from LIGO-Virgo binaries – To calculate the GW foreground generated by the unresolvable BBH, we subtract from the total GW energy density emitted by all the binaries the contribution from those that are sufficiently loud to be seen individually. The GW foreground then is different for different detectors, and its dimensionless energy density is

$$\Omega_{\text{BBH}}(f) = \int \frac{dV_c}{1+z} dR(z) \frac{1}{\rho_c} \frac{d\rho_{\text{GW}}}{df} [1 - p_{\text{det}}(f)], \quad (10)$$

where dV_c is the differential comoving volume element at redshift z , ρ_c is the critical energy density of the Universe, $d\rho_{\text{GW}}$ is the GW energy density emitted by a binary in the frequency range $(f, f + df)$ [31],¹

$$d\rho_{\text{GW}} = \frac{4}{5} \frac{\pi}{G} f^3 |\tilde{h}(f)|^2 df, \quad (11)$$

dR denotes the differential BBH merger rate (1), and the factor $1 - p_{\text{det}}(f)$ removes the binaries that are individually resolvable within the duration of the given experiment.

¹ Here the factor $4/5$ accounts for the average over source orientations.

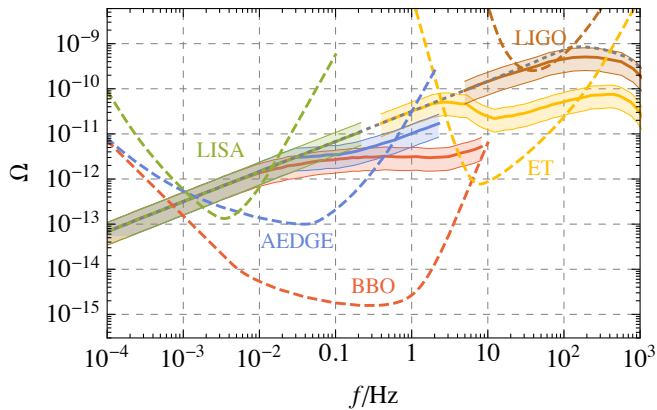


FIG. 2. Solid curves show the central value of the GW foreground from unresolvable BH binaries for different observatories, while the colorful bands indicate their uncertainties stemming from uncertainty on BBH merger rate. Dashed curves show the reach of the corresponding observatories in terms of power-law integrated sensitivities, and the gray dashed curve indicates the total GW energy density emitted by the BH population.

In Fig. 2 we show the GW foreground from unresolvable BBHs for different GW experiments. The solid curves in Fig. 2 indicate the foreground calculated with the central value of R_0 . Since $\Omega_{\text{BBH}} \propto R_0$ the boundaries of the 1σ band on the BBH foreground can be obtained simply by multiplying the result obtained using the central value of R_0 by 1.6 (upper boundary) or 0.5 (lower boundary). The gray dotted curve in Fig. 2 indicates the total GW foreground before any binaries are resolved, obtained by taking $p_{\text{det}} \rightarrow 0$ in Eq. (10). At $f \lesssim 10$ Hz this curve is simply a power-law, $\Omega_{\text{BBH}} \propto f^{2/3}$. In Fig. 1 the BBH strain curve corresponds to the total BBH foreground calculated with the central value of R_0 . This is what we use as the BBH contribution to the instantaneous noise in the detector.

The dashed curves in Fig. 2 show the standard power-law integrated sensitivities [32] of the experiments, which account for the foregrounds only in the instantaneous detector noise. The signal-to-noise ratio of the GW background is given by

$$\text{SNR}_{\text{BG}} = \sqrt{\mathcal{T} \int df \left[\frac{\Omega_{\text{GW}}(f)}{\Omega_n(f)} \right]^2}, \quad (12)$$

and the power-law integrated curves are obtained as the envelope of the power-laws that give $\text{SNR}_{\text{BG}} = \text{SNR}_c = 8$. The detector noise is the sum of the instrumental noise, and the GW foregrounds from BWDs and BBHs, $\Omega_n(f) = \Omega_{\text{instr}}(f) + \Omega_{\text{BWD}}(f) + \Omega_{\text{BBH}}(f)$. Notice that, just as in Eq. (6), $\Omega_{\text{BBH}}(f)$ is the total BBH foreground before any binaries are resolved.

Detectability of a GW background – To study the impact of the BBH foreground on the detectability of the

GW background, we estimate how accurately the background can be measured using Fisher analysis. The total stochastic noise in the GW detector is given by the sum of the GW background, which we model as a power-law, the WBD and the BBH foregrounds, and the instrumental noise,

$$\Omega_{\text{GW}}(f) = \Omega \left(\frac{f}{f_{\text{ref}}} \right)^\alpha + A \langle \Omega_{\text{BBH}}(f) \rangle + \Omega_{\text{BWD}}(f) + \Omega_{\text{instr}}(f), \quad (13)$$

where Ω is the amplitude of the GW background at a reference frequency f_{ref} , α is the spectral index of the GW background, and $A \langle \Omega_{\text{BBH}}(f) \rangle$ is the contribution from unresolvable BBHs. We calculate $\langle \Omega_{\text{BBH}}(f) \rangle$ using the central value for the present merger rate, $\langle R_0 \rangle = 10 \text{ Gpc}^{-3} \text{ yr}^{-1}$, and we have introduced the parameter $A = R_0 / \langle R_0 \rangle$ to account for the uncertainties in the amplitude of the BBH foreground. Our main aim is to demonstrate the impact of the BBH foreground on the detectability of a GW background and for the sake of clarity we don't include the uncertainties in the BWD foreground or in the instrumental noise in our analysis. Moreover, while simultaneously utilizing data from multiple experiments would improve the prospects of detecting cosmological GW backgrounds [33], for simplicity we consider each of the experiments individually.

The variances of the model parameters can be estimated from the inverse of the Fisher matrix, whose ij component is given by

$$\Gamma_{ij} = \mathcal{T} \int df \frac{\partial_i \Omega_{\text{GW}}(f) \partial_j \Omega_{\text{GW}}(f)}{\Omega_n(f)^2}, \quad (14)$$

as

$$\sigma_j^2 = \Gamma_{jj}^{-1}. \quad (15)$$

Calculating the Fisher matrix only in Ω we get

$$\frac{\sigma_\Omega}{\Omega} = \sqrt{\Omega^{-2} \Gamma_{\Omega\Omega}^{-1}} = \text{SNR}_{\text{BG}}^{-1}, \quad (16)$$

which shows that the amplitude of any power-law that touches the power-law integrated sensitivity curve can be measured with accuracy $\sigma_\Omega / \Omega = \text{SNR}_c^{-1}$, assuming that the spectral index α and the BBH foreground are known with negligible uncertainties.

Next we aim to find a curve similar to the power-law integrated one, which takes into account the uncertainties in the BBH foreground. In the fashion of the power-law integrated sensitivity, this curve does not include the information of the accuracy at which the spectral index of the power-law GW background spectrum can be determined. We find this curve by performing a Fisher analysis in Ω and A for different fixed values of α (see eq. (13)). We account for the measured uncertainties in

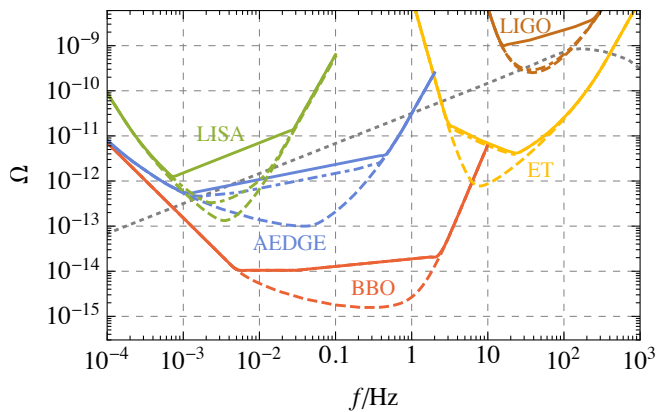


FIG. 3. Solid and dot-dashed curves show the sensitivities on GW background accounting for the BBH foreground with the prior $\sigma_{A,0} = 0.6$ and $\sigma_{A,0} = 0.06$, respectively. Dashed curves show the power-law integrated sensitivities as in Fig. 2.

the present BBH merger rate R_0 by setting a prior on A by the replacement

$$\Gamma_{AA} \rightarrow \Gamma_{AA} + 1/\sigma_{A,0}^2. \quad (17)$$

We use $\sigma_{A,0} = 0.6$, which arises from the 1σ upper bound on the present merger rate $R_0 < 16 \text{ Gpc}^{-3} \text{ yr}^{-1}$.

The solid curves in Fig. 3 show the sensitivities of different experiments obtained as described above by requiring that $\sigma_{\Omega}/\Omega < \text{SNR}_c^{-1}$. In the same way as the power-law integrated curve, the curves shown in Fig. 3 depict the envelope of different power-laws that are detectable. As expected, these curves lie above the power-law integrated sensitivity curves. The effect is particularly strong for LIGO, LISA and AEDGE, whereas ET and BBO can probe the GW background well below the BBH foreground. The reason is that ET and BBO will be able to measure the BBH foreground very accurately. This means also that changing the prior of A does not significantly change the sensitivity prospects for these experiments. Instead, for LISA and LIGO more accurate measurement of the BBH merger rate will greatly improve the prospects for probing GW background. We show this by the dot-dashed curves that are calculated assuming an order of magnitude improvement in the accuracy of the BBH merger rate, which would imply $\sigma_{A,0} = 0.06$. For LIGO this curve overlaps with the power-law integrated sensitivity, whereas for BBO and ET it overlaps the curve obtained with the current accuracy on the rate, $\sigma_{A,0} = 0.6$.

Fig. 3, however, does not give a completely accurate picture of the prospects for the detectability of the GW background. While any power-law that touches the sensitivity curves shown in Fig. 3 can be detected, for example with LISA assuming $\sigma_A = 0.6$ a flat GW background can be detected even if it doesn't touch the solid green curve. As the foreground for LISA is a power-law with spectral

index $2/3$, detecting a GW background with $\alpha = 2/3$ requires a larger amplitude, and therefore that power-law cuts the sensitivity curve for LISA in Fig. 3. The minimal detectable amplitude for a given value of α can be more clearly read from Fig. 4. The amplitudes for each experiment in these plots are given at a reference frequency that roughly corresponds to the best power-law sensitivity of the experiment.

Finally, for an easy comparison of different cases, we have collected in Table I the values of minimal detectable amplitude of a flat, $\alpha = 0$, GW background. In this table we show the result also in the case that the uncertainties in α are accounted for in the Fisher analysis. This is denoted with $\sigma_{\alpha,0} \rightarrow \infty$, and the case where α is fixed is denoted by $\sigma_{\alpha,0} \rightarrow 0$. In practice, in the latter case we calculate the Fisher matrix only in Ω and A , whereas in the former case we calculate it in Ω , A and α . When α is included in the Fisher analysis, the result depends also on the reference frequency f_{ref} . In Table I the reference frequencies for each experiment are fixed in the same way as in Fig. 4. In all cases the minimal detectable amplitude of the GW background is determined by requiring that $\sigma_{\Omega}/\Omega < \text{SNR}_c^{-1}$. For the first row in the table we assume that the foreground is known and calculate the Fisher matrix only in Ω . As described above, this corresponds to the usual power-law integrated result.

Conclusions – We have analysed the impact of the population of compact objects currently probed by LIGO-Virgo on future searches for a stochastic GW background of primordial origin. The GW foreground associated with the current observations has not been probed directly yet. However, the rate of events inferred by the LIGO-Virgo observations suggests that it will have a large amplitude, and will cut significantly into the integrated sensitivities of upcoming detectors limiting their reach. We improved the modeling of the foreground for each experiment using the fact that the binaries identified with a large SNR can be subtracted. The impact of this procedure can be different across the frequency range for any given experiment as the binaries at low frequencies are typically in the inspiral phase which can last much longer than the duration of the experiment. Thus, the time integrated SNR is much smaller than one would expect simply looking at the frequency spectra for such binaries. This leads to more difficult identification and smaller foreground subtraction at lower end of the frequency spectrum of many experiments.

To assess the impact of the astrophysical foreground on future searches for a primordial stochastic GW background including our improved modeling we use Fisher matrix analysis. Describing the primordial background as a power-law with a given slope, we check what amplitudes could be probed in the presence of the foreground with each experiment. We find the impact to be much smaller than one would expect from simply looking at the

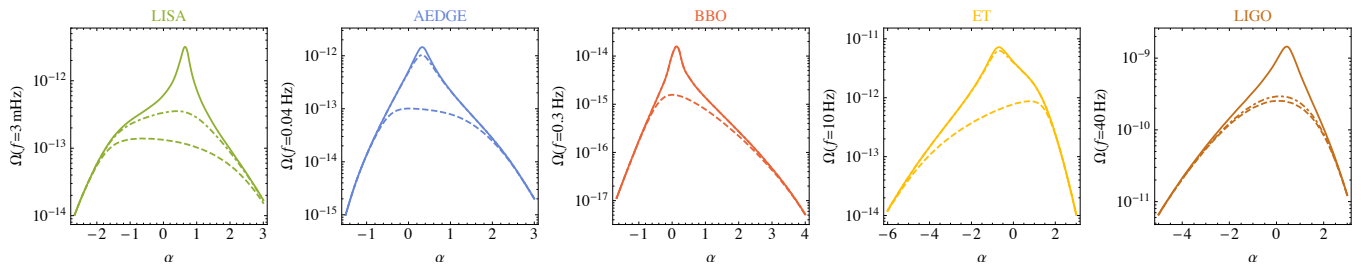


FIG. 4. Minimal detectable amplitude of the power-law GW background as a function of its spectral index α . The solid and dot-dashed curves include the BBH foreground with the current and an order of magnitude improved accuracy of the BBH merger rate, respectively. The dashed curves correspond to the usual power-law integrated sensitivities.

$\sigma_{A,0}$	$\sigma_{\alpha,0}$	LISA	AEDGE	BBO	ET	LIGO
0	0	1.3×10^{-13}	9.9×10^{-14}	1.6×10^{-15}	7.6×10^{-13}	2.5×10^{-10}
	∞	1.4×10^{-13}	1.0×10^{-13}	1.6×10^{-15}	1.0×10^{-12}	2.5×10^{-10}
0.06	0	3.3×10^{-13}	4.6×10^{-13}	1.0×10^{-14}	3.9×10^{-12}	2.9×10^{-10}
	∞	3.5×10^{-13}	1.3×10^{-12}	2.3×10^{-14}	5.1×10^{-12}	3.0×10^{-10}
0.6	0	5.9×10^{-13}	4.8×10^{-13}	1.0×10^{-14}	4.0×10^{-12}	9.3×10^{-10}
	∞	2.0×10^{-12}	3.3×10^{-12}	2.3×10^{-14}	5.4×10^{-12}	1.5×10^{-9}

TABLE I. Minimal detectable amplitude Ω of a flat ($\alpha = 0$) GW background. The first two columns show the priors used for the relative amplitude A of the BBH foreground and the spectral index α of the GW background.

amplitude of the foreground, especially for instruments that can themselves probe the foreground accurately. Instead for instruments unable to significantly improve the foreground measurement the final result depends on our prior knowledge. We illustrate this showing also results assuming the accuracy of the BBH merger rate improved by an order of magnitude which in the case of LISA and LIGO significantly alleviates the problem, while giving almost negligible change in AEDGE, BBO and ET. However, the impact remains vital and while subtraction of loud identifiable binaries helps, the sensitivity of all future experiments in terms of the abundance of the primordial background they can reach is lowered in each case.

Acknowledgments – This work was supported by the Spanish MINECO grants FPA2017-88915-P and SEV-2016-0588, the Spanish MICINN (PID2020-115845GB-I00/AEI/10.13039/501100011033), the grant 2017-SGR-1069 from the Generalitat de Catalunya, the Polish National Science Center grant 2018/31/D/ST2/02048, and the Polish National Agency for Academic Exchange within Polish Returns Programme under agreement PPN/PPO/2020/1/00013/U/00001. IFAE is partially funded by the CERCA program of the Generalitat de Catalunya.

* marek.lewicki@fuw.edu.pl

† vvaskonen@ifae.es

- [1] C. Caprini and D. G. Figueroa, *Class. Quant. Grav.* **35**, 163001 (2018), arXiv:1801.04268 [astro-ph.CO].
- [2] R. Abbott *et al.* (LIGO Scientific, Virgo, KAGRA), *Phys. Rev. Lett.* **126**, 241102 (2021), arXiv:2101.12248 [gr-qc].
- [3] A. Romero, K. Martinovic, T. A. Callister, H.-K. Guo, M. Martínez, M. Sakellariadou, F.-W. Yang, and Y. Zhao, *Phys. Rev. Lett.* **126**, 151301 (2021), arXiv:2102.01714 [hep-ph].
- [4] A. Romero-Rodriguez, M. Martinez, O. Pujolàs, M. Sakellariadou, and V. Vaskonen, (2021), arXiv:2107.11660 [gr-qc].
- [5] B. P. Abbott *et al.* (LIGO Scientific, Virgo), *Phys. Rev. X* **9**, 031040 (2019), arXiv:1811.12907 [astro-ph.HE].
- [6] R. Abbott *et al.* (LIGO Scientific, Virgo), *Phys. Rev. X* **11**, 021053 (2021), arXiv:2010.14527 [gr-qc].
- [7] R. Abbott *et al.* (LIGO Scientific, VIRGO, KAGRA), (2021), arXiv:2111.03606 [gr-qc].
- [8] G. Nelemans, L. R. Yungelson, and S. F. Portegies Zwart, *Astron. Astrophys.* **375**, 890 (2001), arXiv:astro-ph/0105221.
- [9] A. J. Farmer and E. S. Phinney, *Mon. Not. Roy. Astron. Soc.* **346**, 1197 (2003), arXiv:astro-ph/0304393.
- [10] N. Cornish and T. Robson, *J. Phys. Conf. Ser.* **840**, 012024 (2017), arXiv:1703.09858 [astro-ph.IM].
- [11] T. Robson, N. J. Cornish, and C. Liu, *Class. Quant. Grav.* **36**, 105011 (2019), arXiv:1803.01944 [astro-ph.HE].
- [12] T. Regimbau, M. Evans, N. Christensen, E. Katsavounidis, B. Sathyaprakash, and S. Vitale, *Phys. Rev. Lett.* **118**, 151105 (2017), arXiv:1611.08943 [astro-ph.CO].
- [13] Z.-C. Chen, F. Huang, and Q.-G. Huang, *Astrophys. J.* **871**, 97 (2019), arXiv:1809.10360 [gr-qc].
- [14] N. Bartolo, V. Domcke, D. G. Figueroa, J. García-Bellido, M. Peloso, M. Pieroni, A. Ricciardone, M. Sakellariadou, L. Sorbo, and G. Tasinato, *JCAP* **11**, 034

- (2018), arXiv:1806.02819 [astro-ph.CO].
- [15] A. Sharma and J. Harms, Phys. Rev. D **102**, 063009 (2020), arXiv:2006.16116 [gr-qc].
- [16] S. Sachdev, T. Regimbau, and B. S. Sathyaprakash, Phys. Rev. D **102**, 024051 (2020), arXiv:2002.05365 [gr-qc].
- [17] G. Boileau, N. Christensen, R. Meyer, and N. J. Cornish, Phys. Rev. D **103**, 103529 (2021), arXiv:2011.05055 [gr-qc].
- [18] M. Pieroni and E. Barausse, JCAP **07**, 021 (2020), [Erratum: JCAP 09, E01 (2020)], arXiv:2004.01135 [astro-ph.CO].
- [19] K. Martinovic, P. M. Meyers, M. Sakellariadou, and N. Christensen, Phys. Rev. D **103**, 043023 (2021), arXiv:2011.05697 [gr-qc].
- [20] J. Aasi *et al.* (LIGO Scientific), Class. Quant. Grav. **32**, 074001 (2015), arXiv:1411.4547 [gr-qc].
- [21] S. Hild *et al.*, Class. Quant. Grav. **28**, 094013 (2011), arXiv:1012.0908 [gr-qc].
- [22] P. Amaro-Seoane *et al.* (LISA), (2017), arXiv:1702.00786 [astro-ph.IM].
- [23] Y. A. El-Neaj *et al.* (AEDGE), EPJ Quant. Technol. **7**, 6 (2020), arXiv:1908.00802 [gr-qc].
- [24] L. Badurina, O. Buchmueller, J. Ellis, M. Lewicki, C. McCabe, and V. Vaskonen, (2021), arXiv:2108.02468 [gr-qc].
- [25] J. Crowder and N. J. Cornish, Phys. Rev. D **72**, 083005 (2005), arXiv:gr-qc/0506015.
- [26] P. Madau and T. Fragos, Astrophys. J. **840**, 39 (2017), arXiv:1606.07887 [astro-ph.GA].
- [27] K. Belczynski, D. E. Holz, T. Bulik, and R. O’Shaughnessy, Nature **534**, 512 (2016), arXiv:1602.04531 [astro-ph.HE].
- [28] G. Hütsi, M. Raidal, V. Vaskonen, and H. Veermäe, JCAP **03**, 068 (2021), arXiv:2012.02786 [astro-ph.CO].
- [29] P. Ajith *et al.*, Phys. Rev. D **77**, 104017 (2008), [Erratum: Phys.Rev.D 79, 129901 (2009)], arXiv:0710.2335 [gr-qc].
- [30] D. Gerosa, S. Ma, K. W. K. Wong, E. Berti, R. O’Shaughnessy, Y. Chen, and K. Belczynski, Phys. Rev. D **99**, 103004 (2019), arXiv:1902.00021 [astro-ph.HE].
- [31] E. S. Phinney, (2001), arXiv:astro-ph/0108028.
- [32] E. Thrane and J. D. Romano, Phys. Rev. D **88**, 124032 (2013), arXiv:1310.5300 [astro-ph.IM].
- [33] B. C. Barish, S. Bird, and Y. Cui, Phys. Rev. D **103**, 123541 (2021), arXiv:2012.07874 [gr-qc].